Observation of Hydrogen-Ordered Cubic Ice Thin Films on the Surface of Ice Ic Nanocrystals upon Coarsening

*Akira Kouchi[1], Tomoya Yamazaki[1], Hiroyasu Katsuno[1], Hiroki Nada[2], Tetsuya Hama[3], Yuki Kimura[1]**

[1]Institute of Low Temperature Science, Hokkaido University, Sapporo, Hokkaido 060-0819, Japan

[2]Department of Engineering, Tottori University, Tottori, 680-8522, Japan

[3]Komaba Institute for Science, The University of Tokyo, Meguro, Tokyo 153-8902, Japan

ABSTRACT

Ice is ubiquitous, and it has the unique characteristic of exhibiting many polymorphs. Although the rich polymorphism of water ice is due to the existence of hydrogen-order–disorder phases, the order–disorder transition of ice Ic remains unresolved. Through cryogenic transmission electron microscopy, we observed annealing process of ~50-nm sized ice Ic islands on an amorphous SiN substrate at 100-130 K. Water molecules diffused freely on the surface of ice Ic and amorphous SiN under this condition, resulting the coarsening of islands. We found that ~10 nm thick hydrogen-ordered cubic ices grew on the surface of ice Ic islands during coarsening. There might be hydrogen-ordered cubic ices on the surface of ice Ic in various objects in space.

KEYWORDS: Ice Ic, Hydrogen-ordering, Coarsening, Cryogenic Transmission electron microscopy, Electron diffraction.

INTRODUCTION

Water ice is one of the most abundant solid materials in the universe. It is ubiquitous on the Earth and icy bodies of the outer solar system. A unique characteristic of water ice is that it has many polymorphs. Currently, approximately 20 water ice polymorphs have been experimentally confirmed depending on pressure and temperature,[1-6] and this number will soon increase because more structures have been predicted by computational studies[7,8]. The rich polymorphism of water ice is due to the existence of hydrogen-order–disorder phases with identical oxygen lattice structures. Pauling discovered residual entropy for hexagonal ice I (ice Ih), which is a stable phase under atmospheric pressure at low temperatures, and the arrangement of hydrogen atoms in ice Ih is disordered. The hydrogen-ordered form of ice Ih is called ice XI. The formation of ice XI via KOH doping and annealing of ice Ih at approximately 70 K was reported.[9-11] A previous study discovered the formation of ice XI via irradiation of cubic ice I (ice Ic) with high-energy electrons at 95 K.[12] However, the formation of ice XI without a dopant or irradiation has not been achieved despite much active research, and the order–disorder transition of hydrogen atoms in ice crystals can facilitate the understanding of the polymorphism of water ice.

Compared with ice Ih, little is known of the hydrogen-ordered form of metastable ice Ic.[13-20] The structural difference between ice Ih and ice Ic lies in the stacking sequence of the oxygen lattices (wurtzite vs. diamond), and ice Ic exhibits a disordered arrangement of hydrogen atoms. Only two experimental studies (heat capacity measurement of ice Ic and infrared (IR) spectroscopy of KOH-doped ice Ic) have been performed on hydrogen-ordered cubic ice.[14,21] No diffraction study has been performed on hydrogen-ordered cubic ice because large amount of crystals (typically 1 cm^3) are indispensable in the identification of hydrogen-ordered ice by neutron diffraction. Recently, we developed an ultrahigh vacuum cryogenic transmission

electron microscope that enables electron diffraction of nanocrystals.[22] Here, we demonstrated that hydrogen-ordered cubic ice was formed by simply annealing ice Ic islands on a substrate in the range of 100–130 K without a dopant, indicating that the order–disorder transition might be higher than 130 K. The pressure and temperature conditions used were similar to those in interstellar space. Therefore, our results strongly suggested that interstellar ice could exhibit hydrogen-ordered forms when annealed after the formation of a protostar.

EXPERIMENTAL METHODS

We developed an ultrahigh vacuum transmission electron microscope, and the details are described elsewhere.[22] Briefly, a column of the microscope was evacuated using five ion pumps. The pressure measured using a nude ionization gauge mounted between the column and ion pump was ~1×10^{-6} Pa. The partial pressure of H_2O measured using a quadrupole mass spectrometer was ~3×10^{-8} Pa. Considering that the specimen was surrounded by a liquid nitrogen shroud, the total pressure and partial pressure of H_2O near the specimen were maintained lower than the measured values. The sample specimen was cooled using a Gatan ULTST cooling holder. Although this holder was originally made for liquid He use, we used liquid N_2. The minimum temperature attained was approximately 70 K, and the duration of observation was approximately 1 and 6 h at 70 and 130 K, respectively. This is because the lower the temperature, the more liquid-N_2 must flow to maintain the temperature. One of three ICF 70 ports directed at the surface of the specimen at an incident angle of 55° was used for ice deposition, and a Ti gas inlet tube with a 0.4-mm inner diameter faced the substrate. The other two ports were used for an ultraviolet (UV) lamp (30-W D_2 lamp, Hamamatsu, L7293) and the quadrupole mass spectrometer (ULVAC, BGM2-101). Before setting the lamp for transmission electron microscopy (TEM), the UV flux was measured to be ~2×10^{13} photons cm^{-2} s^{-1} using

another vacuum chamber. The UV rays from the D_2 lamp were collimated using a mirror-finished pure Al collimator.

A previous study observed UV-induced formation of ice XI *in situ* using an extremely weak electron beam (~6×10^{-3} electrons $Å^{-2}$ s^{-1} at the sample position, 20000×) with an accelerating voltage of 80 kV.[22] However, we observed that the electron diffraction spots of hydrogen-ordered cubic ice were too weak to be detected. Therefore, we used an approximately 20 times stronger electron beam (0.1 electrons $Å^{-2}$ s^{-1} = 10^{15} electrons cm^{-2} s^{-1} at the sample position, 20000×). Notably, the intensity of the electron beam was still weaker than that in the usual TEM observation, and we could not observe any image on the fluorescent screen. To avoid electron beam damage, we operated in the low magnification mode (20000–30000×) using a charge-coupled device (CCD) camera (Gatan, ES500W). The electron diffraction patterns were collected in the central 700-nm circular region, including approximately 20 crystals, with an exposure time in the range of 180–300 s. In these conditions, we could not obtain an ideal powder diffraction pattern, and the intensity of strong diffraction spots was saturated. Therefore, we did not perform detailed crystal structure analysis as usually performed in the structural analysis of ice crystals by X-ray or neutron powder diffraction.

Ice Ic was deposited at 140 K on 5-nm-thick amorphous SiN films (SiMPore Inc., SN100-A05Q33A). We could not precisely estimate the thickness of the ice samples because the sticking coefficient of H_2O vapor on the substrate was not unity under a pressure of ~1×10^{-6} Pa[23] and because the samples were not uniform films but three-dimensional islands. Roughly, the thickness of the ice Ic islands might be approximately 50 nm, resulting in a deposition rate of 50 nm/10 min. After deposition, the samples were cooled to the desired temperature range of 83–130 K. We performed three systematic experiments: annealing, UV irradiation, and long-term

electron irradiation. In the first two, observations were made at completely different sites of the sample to avoid long-term (>5 min) electron beam irradiation. During electron irradiation, conversely, the irradiation and observation area was limited to 6 × 6 μm^2 to investigate the effect of electron irradiation. In addition, we performed slow deposition at 120 K and crystallization of amorphous ice at 130 K. For all experiments, the diameter of the electron beam was approximately 10 μm. The durations of the observations at 130 and 83 K were 6 and 2 h, respectively.

To identify the phase of the produced ice, d-spacings (d) and relative intensities of peaks in electron diffraction from hydrogen-ordered cubic and hexagonal ices were calculated based on the lattice model proposed by Raza et al.[18], which provided 11 structures of hydrogen-ordered cubic ice (C1–C11) and 16 structures of hydrogen-ordered hexagonal ice (H1–H16) using the Recipro program.[24] C1–C11 and H1–H16 correspond to the structure numbers in a previous study.[18] According to the definition of the unit cell for C1-C11 by Raza et al., the unit cell is $2 \times 1 \times 1$ supercell of tetragonal cell which is created by cutting through the (011) plane of hydrogen-disordered cubic ice. The resultant unit cell is orthorhombic cell with $\sqrt{2}a \times \sqrt{2}\,a/2 \times a$, where a is the side length of hydrogen-disordered cubic ice.[18] For hexagonal ice, orthorhombic cell with $\sqrt{2}a \times \sqrt{6}a \times 4\sqrt{3}a/3$ constructed by Hirsch and Ojamäe was used.[21] The actual value of lattice constants of each structure used for calculations were listed in Table S1, and these were slightly different because of relaxation operations.[18]

The program can calculate relative intensities and reproduce electron diffraction patterns using lattice parameters, atom types, and atom positions. In this calculation, the space group for all ordered phases was defined as $P1$ to exclude the symmetry constraints (reflection conditions arising from the symmetry of the space group were not included in the data). We used the

relaxed structure data of lattice parameters (Table S1) and all atomic positions (8 oxygen and 16 hydrogen atoms) of each ordered phase.[18] The calculation results for C1-C11 were summarized in Table 1 and for readability of the table, *d* was normalized so that the highest value of *d*, which corresponds to hkl~111 in ice Ic, was 3.68 Å.

For comparison, we also calculated *d* and relative intensities from stacking-disordered forms of ice (ice Isd), which consists of mixed stacking sequences of Ih and Ic. It should be noted that the most of bulk ice Ic observed experimentally in the past might be Isd,[26] and only recently, pure bulk ice Ic has been successfully produced.[27,28] The most characteristic feature of Isd is that the diffraction peak can be found around 3.8 Å, which does not appear in ice Ic.[26] Although various patterns of stacking are possible in Isd, here we have made calculations for several polymorphs (4H, 6H, 9R)[29, 30] with geometrically defining unit cells and atomic positions without relaxing operation. We defined the distance between oxygen atoms was 2.75 Å, and the shorter distance between oxygen and hydrogen atoms was 1.01 Å. The oxygen atoms made tetrahedron and hydrogen positions were disordered. The structure and lattice parameters of Isd was shown in Fig. S1 and Table S1, respectively, and the calculation results of *d* and relative intensities for Isd was listed in Table 2. The listed relative intensities of each set of structures were calculated by normalizing the plane with the strongest reflection intensity as 100. This plane corresponds to that with $d = 3.68$ Å in all structures. Note that the three structures listed here as representatives of ices Isd are still not known to exist as a single crystal. In addition, it will be future work to calculate more realistic relative intensities from the structures with relaxation operations.

Interestingly, the calculated *d* and relative intensities of hydrogen-ordered cubic ice did not match that of the ideal space group (Table 1). For example, the space group of C1 is $I4_1md$, and electron diffraction from the lattice plane with $d = 9.01$ Å, which appears in the calculation,

cannot appear for this space group. The same issue can be seen in the other simulated results though their relative intensities were very weak. This is due to the small difference in atomic positions between the relaxed and ideal structures. It is very interesting that the relaxed structure shows reflections that would not be seen in such an ideal structure. We used the simulated data for discussion because they would be more realistic. To compare with the hydrogen-ordered cubic ice, we referred to the diffraction patterns of ice Ih,[31] ice Ic,[31]. and ice XI which corresponds to H1[18] (Table 2). Regarding hydrogen-ordered hexagonal ice, in addition to H1, only H9 and H11 are shown in Table 2 because of the similarity of the data. Table 2 shows that the diffraction spots of hydrogen-ordered cubic ice corresponding to *d* larger than 4 Å never overlapped with the diffraction spots of ices Isd, ice Ih, ice Ic. In hydrogen-ordered hexagonal ice, *d* = 7.81, 5.36, and 4.50-4.51 Å are greater than 4 Å and overlap with hydrogen-ordered cubic ice at *d* = 4.50-4.51 Å. We also discovered that *d* = 3.19 Å was observed only in hydrogen-ordered cubic ice. Therefore, the d-spacings observed mainly in hydrogen-ordered cubic ice were used to group the polymorphs into Groups A (*d* = 9.01 Å), B (*d* = 6.37 Å), C (*d* = 5.21 Å), D (*d* = 4.51 Å), and E (*d* = 3.19 Å). Hydrogen-ordered cubic ice or hexagonal ice could be identified when one of the diffraction spots belonging to the groups appeared.

Table 1. Calculated relative intensities of hydrogen-ordered ices Ic in electron diffractions

d (Å)	hkl[a]	Group	Structure number and ideal space group										
			C1	C2	C3	C4	C5	C6	C7	C8	C9	C10	C11
			$I4_1md$	$P4_12_12$	$Pna2_1$	$Pna2_1$	$Pmn2_1$	$Pca2_1$	$P2_12_12$	Pc	Pc	$P2_1$	$P2_1$
9.01	100	A	+		+		+	+	+	+		+	+
6.38	001	B		+	+	+	+	+	+	+	+	+	+
5.21	101	C	+	+		+	+	+	+	+	+	+	+
4.51-4.50	200, 010	D	+	+		+	+			+	+	+	+
4.03	110			+		+		+	+	+	+	+	+
3.68	011, 201		+++	+++	+++	+++	+++	+++	+++	+++	+++	+++	+++
3.41	111		+	++	+	+	+	+	+	+	++	+	+

3.19	210, 002	E		+		+	+	+		+	+	+	+
3.01	102, 300		+	+	+	+	+	+	+	+	+	+	+
2.85	211		+	+	+	+	+	+	+	+	+	+	+
2.72	301		+	+	+	+	+	+	+	++	+	++	+
2.60	012, 202			++	+	++	+	+	+	+	++	+	++
2.50	112, 310		+	++	+	+	++	+	+	++	++	++	+
2.33	311		+	+	+	+	++	+	+	++	+	++	+
2.25-2.26	020, 212, 400		+++	+++	+++	+++	+++	+++	+++	+++	+++	+++	+++
2.19	302, 120		+	++	++	+	++	++	++	++	++	++	+
2.12	401, 003, 021		+	++	++	++	++	+	+	++	++	++	++
2.07	103, 121		+	++	+	++	++	++	++	++	++	++	+

The diffraction intensities are grouped according to the calculated relative intensities (%) into +++, 1-100; ++, 0.1-1; and +, 0.001-0.1.

[a]Miller indices for C1-C11.

Table 2. Calculated relative intensities of ices Isd (4H, 6H, 9R), ice XI (~H1), hydrogen-ordered ice Ih (H9 and H11), and referred data by X-ray diffractions.

d (Å)	hkl[a]	Group	C1~11	4H	6H	9R	H1	H9	H11	Ih[b]	Ic[b]
9.01	100	A	+								
7.81								+			
6.38	001	B	+								
5.36									+		
5.21	101	C	+								
4.51-4.50	200, 010	D	+					+			
4.03	110		+								
3.92-3.90				+++			+++	+++	+++	+++	
3.88						+++					
3.84					+++			+			
3.80						+++					
3.77				+++							
3.68	011, 201		+++	+++	+++	+++	+++	+++	+++	+++	+++
3.53						+++					
3.46-3.42				+++	+++		+++	+++	+++	+++	
3.41	111		++								

3.36						+++					
3.33									++		
3.19	210, 002	E	+								
3.05				+++							
3.01	102, 300		+			++					
2.95								+	+		
2.92					+++						
2.85	211		+					+			
2.84						+++					
2.74								+	+		
2.72	301		++								
2.68				+++			+++	+++	+++	+++	
2.60	012, 202		++								
2.53						+++					
2.50	112, 310		++								
2.45					+++			+	+		
2.38						+++					
2.35				+++							
2.34									++		
2.33	311		++								
2.30									+		
2.25-2.26	020, 212, 400		+++	+++	+++	+++	+++	+++	+++	+++	+++
2.19	302, 120		++								
2.17								++	++		
2.15							++	+	++		
2.13						+++					
2.12	401, 003, 021		++						+		
2.08				+++	+++		+++	+++	+++	+++	
2.07	103, 121		++								

The diffraction intensities are grouped according to the calculated relative intensities (%) into +++, 1-100; ++, 0.1-1; and +, 0.001-0.1.

[a]Miller indices for C1-C11.

[b]Measured by X-ray

RESULTS AND DISCUSSION

The changes in the TEM images and electron diffraction patterns during annealing at 120 K are shown in Figure 1A and B. The ice crystals deposited at 140 K and cooled to 120 K were discrete three-dimensional (3D) islands and were uniformly approximately 50 nm in size. Thereafter, the islands coarsened. As shown in Figure 1B, the initial ice was ice Ic, and many diffraction spots appeared with time, which did not correspond to ice Ih or XI. A similar change in the electron diffraction pattern was observed when cooled to 130 K, but no such change was observed when cooled to 83 K. Ice Ic sometimes includes ice Isd.[26,32] When stacking-disordered ice is included, the electron diffraction pattern shows some streaks, as shown in Figure 2 and the literature (Figure 3 in reference[12] and Figure 8 in reference[22]). However, we did not observe any streaks in our ice Ic samples. The density of streaks in these samples decreases in the following order: Figure 3 in reference[12] > Figure 2b in reference[12] > Figure 2 of this paper >> all starting ice Ic in this study. Therefore, we considered the fraction of ice Ic in our sample to be significant.

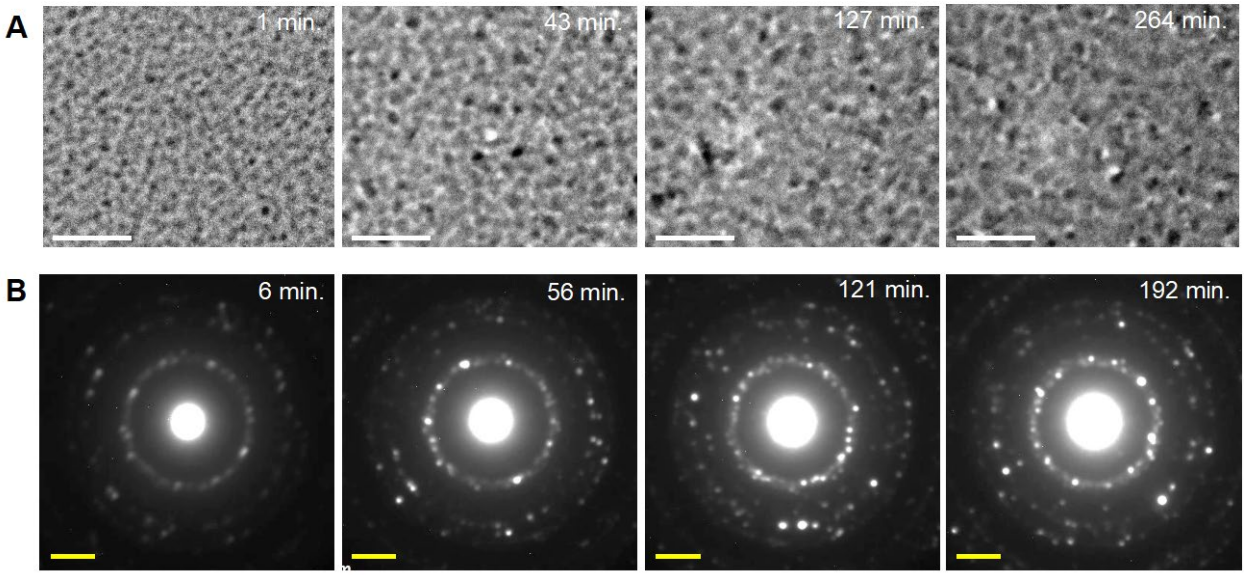

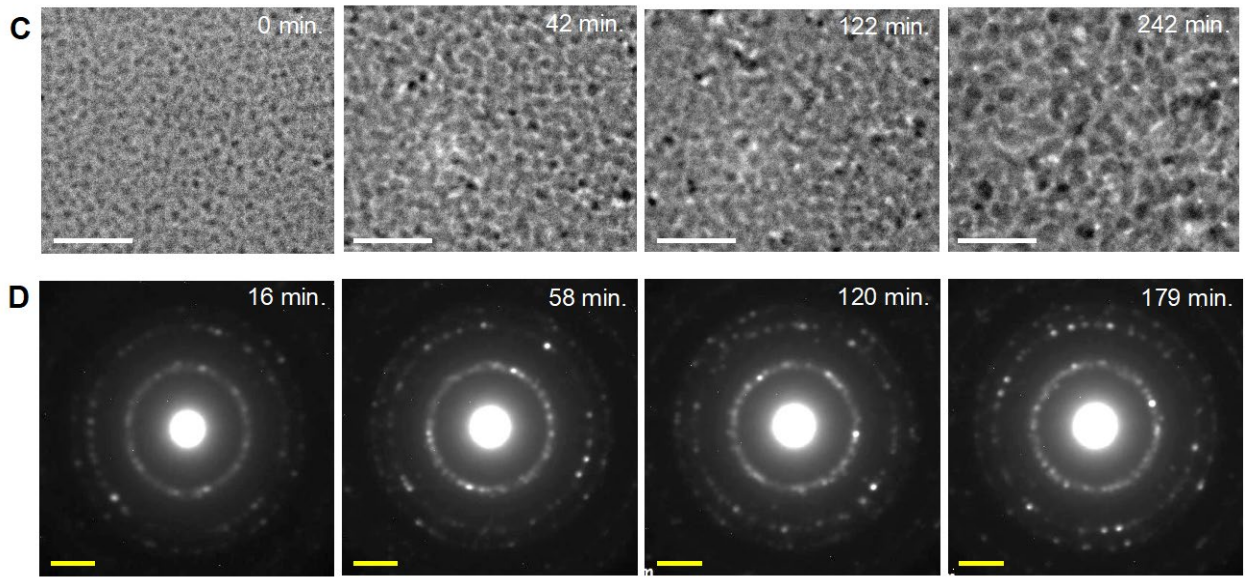

Figure 1. *In situ* TEM observation of annealing and electron irradiation experiments. Changes in TEM images and electron diffraction patterns during annealing (A, B) and electron irradiation (C, D) at 120 K. In annealing experiments (A, B), observations were made at completely different sites of the sample to avoid electron beam irradiation. During electron irradiation, conversely, the irradiation and observation area was limited to 6 × 6 μm^2 to investigate the effect of electron irradiation. The elapsed time is shown in each figure. White scale bars, 500 nm; yellow scale bars, 2 nm^{-1}.

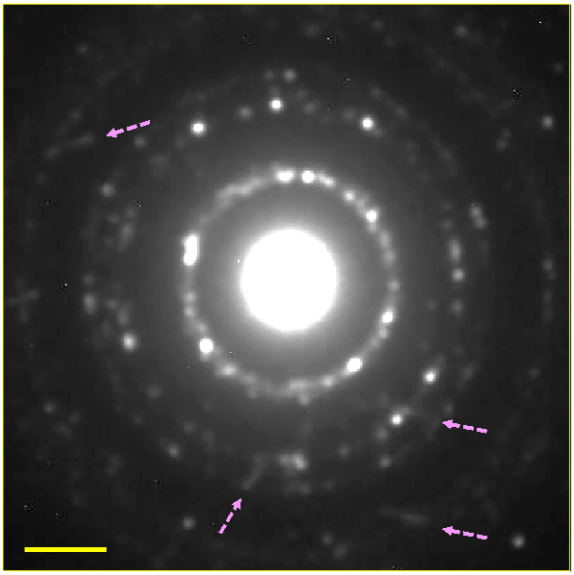

Figure 2. Electron diffraction pattern of an ice sample after 123 min of annealing of ice Ic at 130 K. Some streaks caused by the formation of stacking faults, shown by pink broken arrows, were observed. The possibility of the observation of stacking faults is very small, <0.01. Therefore, we considered that the fraction of ice Isd in the initial ice Ic is very small. Yellow scale bars, 2 nm^{-1}.

From Table 1 and 2, there were no diffraction spots at $d > 4$ Å and $d = 3.19$ Å except for those corresponding to the hydrogen-ordered cubic (and hexagonal) ice polymorphs. Therefore, we identified hydrogen-ordered ice polymorphs when these diffraction spots were observed. Figure 3 shows some of the diffraction spots observed in this study. We observed many diffraction spots belonging to Group A, B, C, and E, which are only observed in hydrogen-ordered cubic ice. Group E ($d = 3.19$ Å) was the most frequently observed polymorphs and appeared throughout the annealing experiment. Groups B ($d = 6.38$ Å) and C ($d = 5.21$ Å) were observed in the middle to later stages. Group A ($d = 9.01$ Å), which contains the most stable polymorph of hydrogen-ordered cubic ice (space group: $I4_1md$), was observed only in the final stage. The ratio observed in the annealing experiments, Group A:Group B:Group C:Group E, was obtained in the following manner. The number of diffraction spots in Groups A-E were counted in several

experiments at each annealing temperature. These appearances were summed for all experiments at all temperatures from 100-130 K. We found that the ratio was Group A:Group B:Group C:Group E = 3:6:13:78. Thus, several hydrogen-ordered cubic ices were formed by simply annealing nondoped hydrogen-disordered ice Ic within 120–130 K. A study on annealing of KOH-doped ice Ic at 70 K suggested that the formed hydrogen-ordered cubic ice might be in a thermodynamically metastable phase with space group $Pna2_1$.[14] Although their assignment using IR spectra was not unique, their suggestion correlated with our observation.

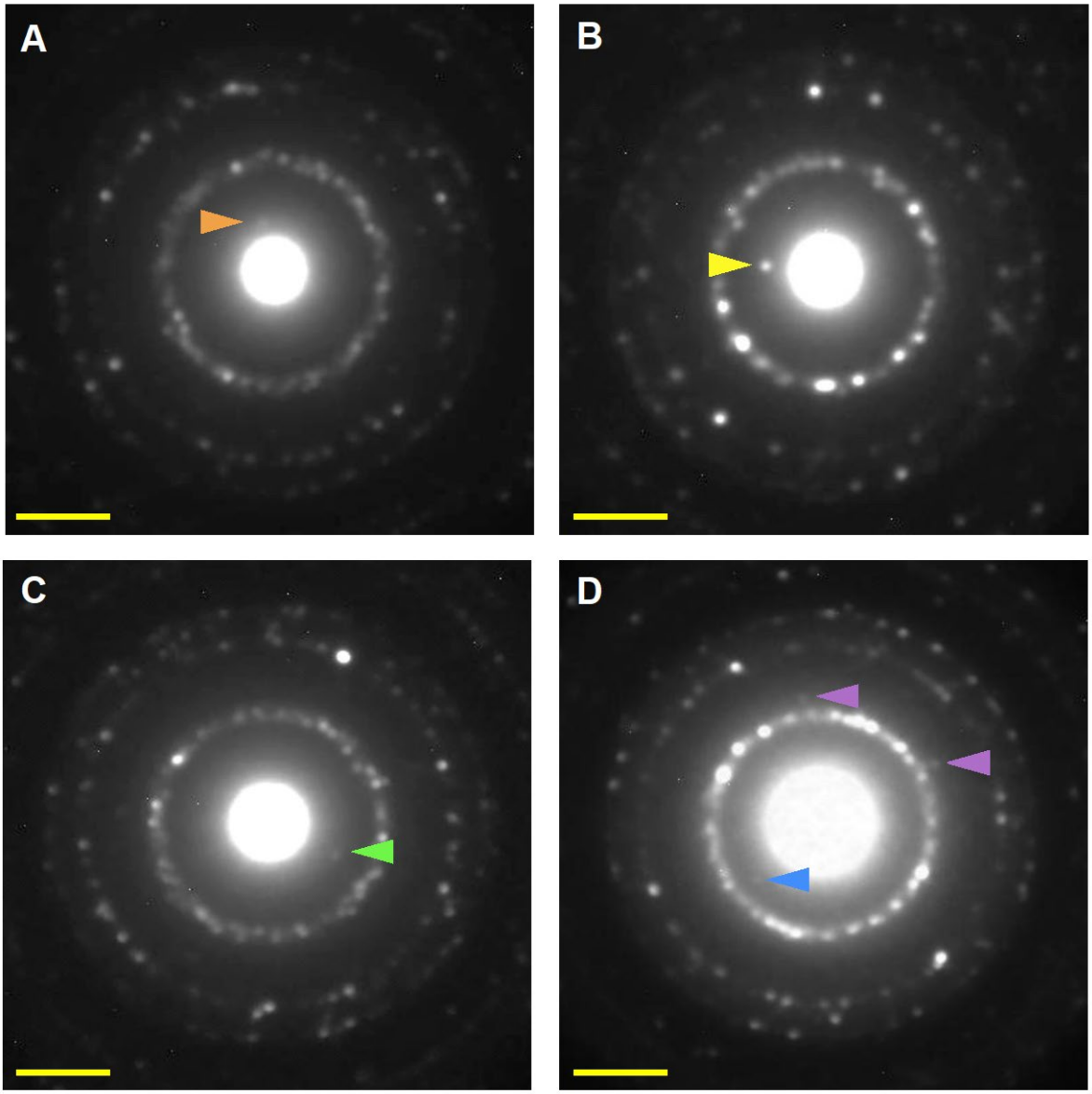

Figure 3. Identification of hydrogen-ordered cubic ices by electron diffraction. Electron diffraction patterns of hydrogen-ordered cubic ice formed by UV irradiation of ice Ic at 120 K for 370 min (A), annealing of ice Ic at 130 K for 342 min (B), annealing of ice Ic at 130 K for 327 min (C), and UV irradiation of ice Ic at 100 K for 61 min (D). Orange, yellow, green, blue, and purple arrowheads show the diffraction spots of Groups A (d = 9.01 Å), B (d = 6.38 Å), C (d = 5.21 Å), D (d = 4.51 Å), and E (d = 3.19 Å) of hydrogen-ordered cubic ice, respectively. Yellow scale bars, 2 nm^{-1}.

The change in the number density of the islands at various annealing temperatures (Figure 4) showed that coarsening rapidly proceeded at high temperatures. The number density decreased with time (A) depending on the temperature. An activation process with activation energy E_a was assumed, and the time was rescaled by $\exp(E_a/kT)$, where k is the Boltzmann constant. The universal function obtained in (B) showed that the power of the function changed in our experimental data. E_a was observed to be approximately 1000 K, probably related to the interfacial incorporation process. The activation energy of surface diffusion of water molecules on the a-SiN substrate was approximately 2000 K (Figure S2). Therefore, the interfacial incorporation process was not the rate-determining process during coarsening.

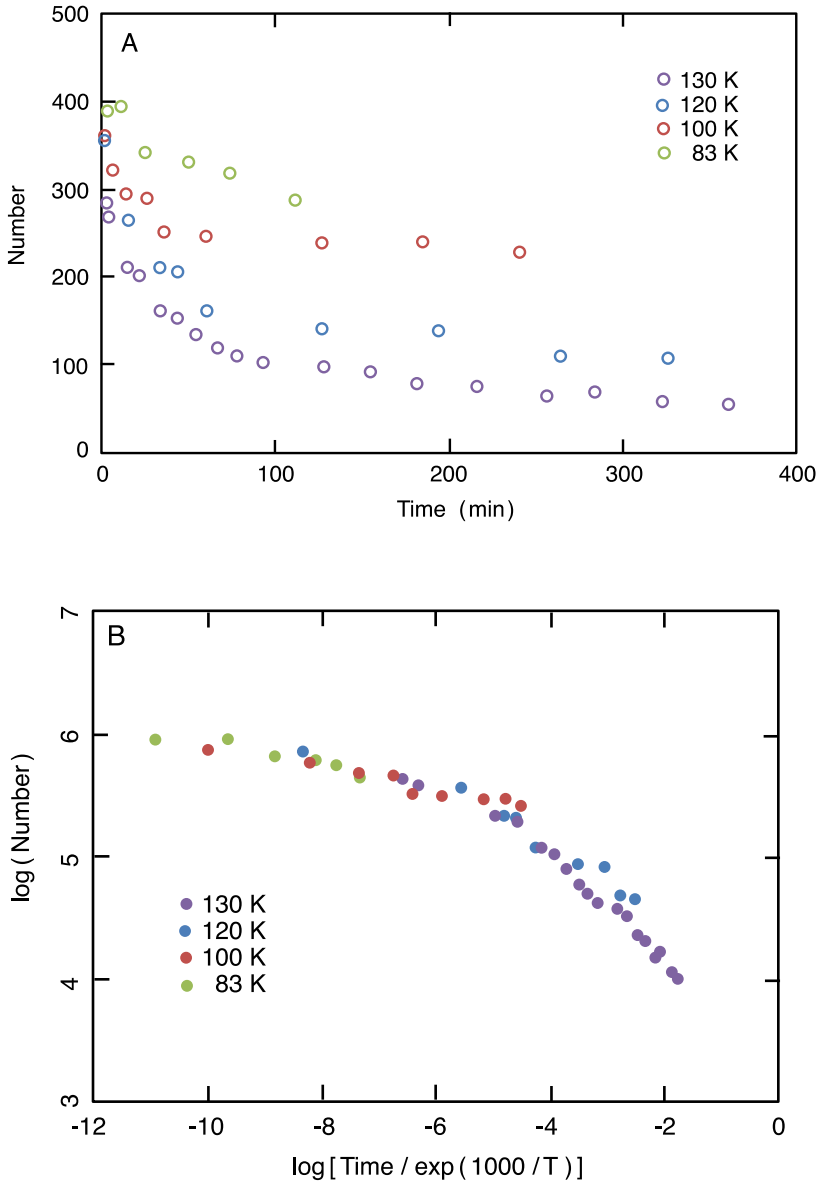

Figure 4. Evolution of the number density of the islands as a function of the annealing time within 83–130 K, with a linear plot (A) and a log–log plot with the scaled time (B).

Figure 5(A) shows an example of how the diameter, *D*, of a 3D island changes with time during annealing at 120 K. Initially, *D* increases rapidly with time, and approaches a constant value, *D* = 105 nm. Assuming that the shape of the 3D island is as shown in Figure 5(B), the

thickness of the grown surface layer, *h*, can be calculated. It can be seen that the thickness is about 10 nm at an annealing time of 50 minutes and about 15 nm at an annealing time of 200 minutes.

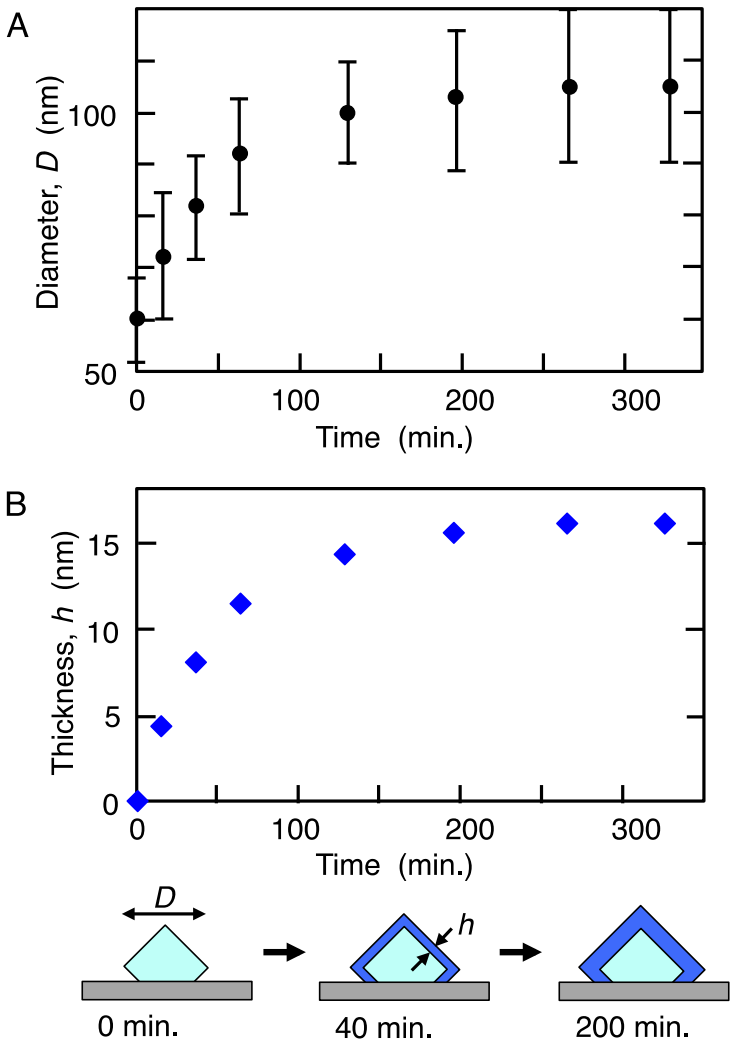

Figure 5. Change of the diameter of islands, *D*, during annealing experiment at 120 K (A). Change of the thickness of the newly grown ice layer, *h*, calculated using the data in A (B). Pale blue: ice Ic; blue: newly grown ice layer.

Figure 6 shows the detection frequency of ice crystal structure obtained from the electron diffraction pattern during annealing experiment. The black dots indicate that only ice Ic was observed. The open green circles indicate that diffraction spots other than ice Ic, Ih, and Isd were observed, indicating the formation of ice with a new structure, but the crystal structure has not been identified. The blue diamonds indicate that diffraction spots of Groups A-E (see Figure 3) were observed, showing the formation of hydrogen-ordered cubic ices. At 120-130 K, the new unidentified ice is observed early (10-20 min.), but at 83-100 K, the new unidentified ice is observed a little later (30-40 min.). Hydrogen-ordered cubic ices were observed after 50 min. at 100-130 K, and the frequency of their appearance increased with time. To clarify this, the fraction of the appearance of hydrogen-ordered cubic ices, obtained from the observed crystal structure data (120 K) in Figure 6, were plotted as a function of thickness (h) as shown in Figure 7. The observed fraction of hydrogen-ordered cubic ice is zero when the thickness is thin, but increases rapidly at thickness larger than 12 nm. This indicates that the fraction of occurrence of hydrogen-ordered cubic ice increases as the thickness of the newly grown ice layer increases, i.e., as coarsening proceeds. It is not clear whether this result indicates that hydrogen-ordered cubic ices formed only in the latter half of coarsening, or a sample with a certain thickness (10 nm) is necessary for the detection of hydrogen-ordered cubic ices by electron diffraction. In ordinary crystals, the minimum thickness for the detection of diffraction spots is about 4 layers. However, to detect diffraction spots of very low intensity (see Table 1), as in hydrogen-ordered cubic ices, a sample of considerable thickness, e.g. 5-10 nm, would be required. Therefore, it is suggested that the latter is the more likely explanation.

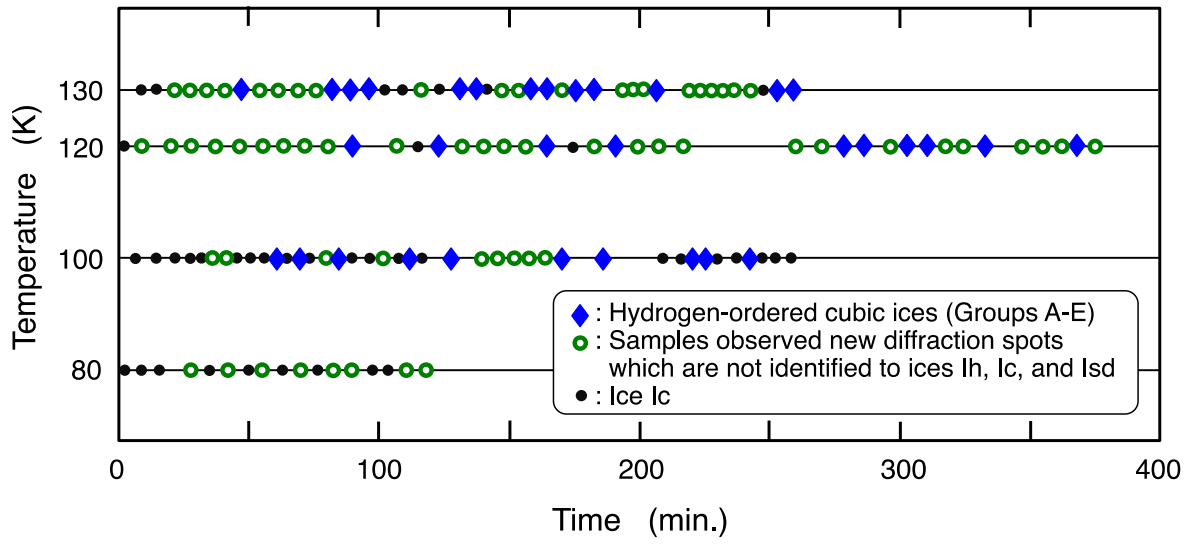

Figure 6. Detection of hydrogen-ordered cubic ices by electron diffraction in annealing experiments. Blue diamonds indicate the presence of at least one diffraction spot in Groups A-E. Green circles indicate new unidentified diffraction spots, which do not correspond to ice Ih, Ic, and Isd. Black dots indicate cases where only ice Ic was detected.

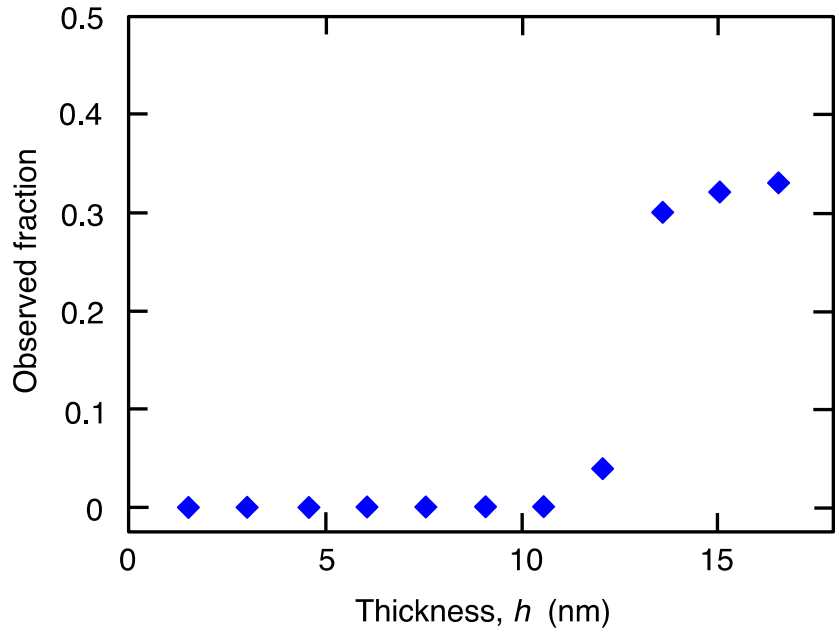

Figure 7. Relationship between the observed fraction of hydrogen-ordered cubic ices and the thickness of the newly grown ice layer, *h*, in the 120 K annealing experiment. The data used are *h* vs. time in Figure 5B, and observed crystal structures vs. time in Figure 6. The moving average of the observed fraction was calculated using two neighboring 3-nm width regions.

Figure 8 shows the temperature dependence of the fraction of the detected hydrogen-ordered cubic ice. During annealing, the fraction was a constant value within 120–130 K, decreased with decreasing temperature, and became zero at 83 K. As already pointed out, the amount of hydrogen-ordered cubic ices formed was related to the degree of coarsening (see Figures 5-7), suggesting that these ices were formed by coarsening. The coarsening indicated that water molecules diffused on the a-SiN substrate and ice Ic. Therefore, hydrogen-ordered cubic ice can be formed without dopants when the conditions for movement of water molecules are satisfied. The measurement of the surface diffusion coefficient of H_2O on a-SiN (Figure S2) supported this conclusion. Furthermore, because we did not observe the formation of a new 3D island on the a-SiN substrate, hydrogen-ordered cubic ice was suggested to epitaxially grow on the hydrogen-disordered ice Ic as shown in the inset of Figure 5B.

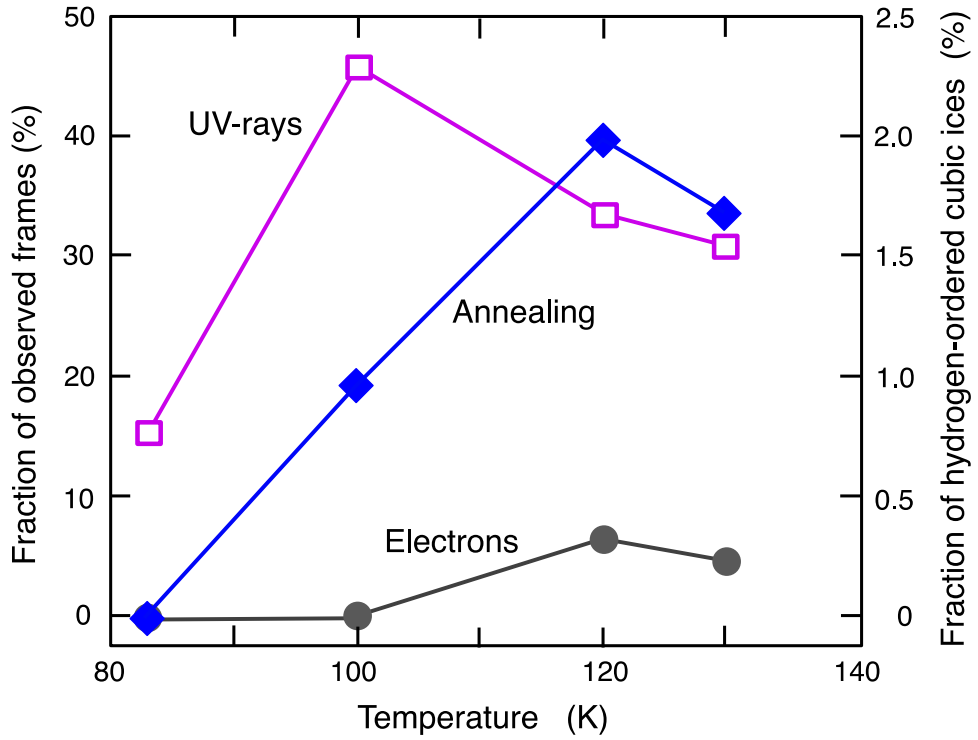

Figure 8. Fraction of identified hydrogen-ordered cubic ices (Groups A-E) vs. temperature after annealing (blue), UV irradiation (purple), and electron irradiation (dark gray). Total numbers of frames observed are as follows: 80 K: 16, 100 K: 36, 120 K: 34, 130 K: 33 in annealing experiments; 80 K: 19, 100 K: 33, 120 K: 38, 130 K: 35 in UV irradiation experiments; and 80 K: 16, 100 K: 18, 120 K: 28, 130 K: 32 in electron irradiation experiments. The fraction in left vertical axis is defined as (number of electron diffraction pattern frames including hydrogen-ordered cubic ices)/(total number of frames observed) and that in right vertical axis as (number of electron diffraction pattern frames including hydrogen-ordered cubic ices)/[(total number of frames observed) × (number of crystals included in the 700-nm circular region in the TEM image)]. Number of electron diffraction pattern frames including hydrogen-ordered cubic ices is obtained from the number of blue diamonds in Figure 6. Notably, the fractions shown in the right vertical axis are the minimum values because we counted only the five groups shown in Figure 3, and because we rarely observed several hydrogen-ordered cubic ices in one frame.

To confirm whether the formation of hydrogen-ordered cubic ice was an effect of the electron beam irradiation used to obtain electron diffraction patterns, although the duration was only 300 s at most, we performed long-term electron beam irradiation of the same position of the sample (Figure 1C and D). The TEM images showed that coarsening proceeded as in the annealing experiments. However, changes were not observed in the electron diffraction pattern of ice Ic, showing that the formation of hydrogen-ordered cubic ice (Figures 1B and 2) was not due to the 300-s electron irradiation and that long-term electron irradiation destroyed rather than formed hydrogen-ordered cubic ice. When hydrogen-ordered cubic ice was detected by electron diffraction, we continuously observed the same position of the sample and discovered that the intensity of the diffraction spots corresponding to the ice occasionally weakened with time (Figure 9). A study showed that hydrogen-ordered cubic ice was not detected under high-energy electron irradiation of ice Ic at 95 K, [12] which correlated with our result. Here, hydrogen-ordered cubic ice was not detected under electron irradiation because the cubic ice formed on the surface of ice Ic was sputtered and/or its entire layer was destroyed. Figure S3 shows a TEM image after 6-h electron irradiation at the same position, showing that sputtering proceeded. Considering that the estimated sputtering rate was ~4 nm/h (Figure S3), the disappearance of certain diffraction spots of hydrogen-ordered cubic ice with 30-min electron irradiation (Figure 9) was suggested to be due to sputtering. This supported the formation of hydrogen-ordered cubic ice on the surface of ice Ic. Therefore, the formation of hydrogen-ordered cubic ice shown in Figures 1B and 2 was not due to the 300-s electron irradiation but to spontaneous phenomena.

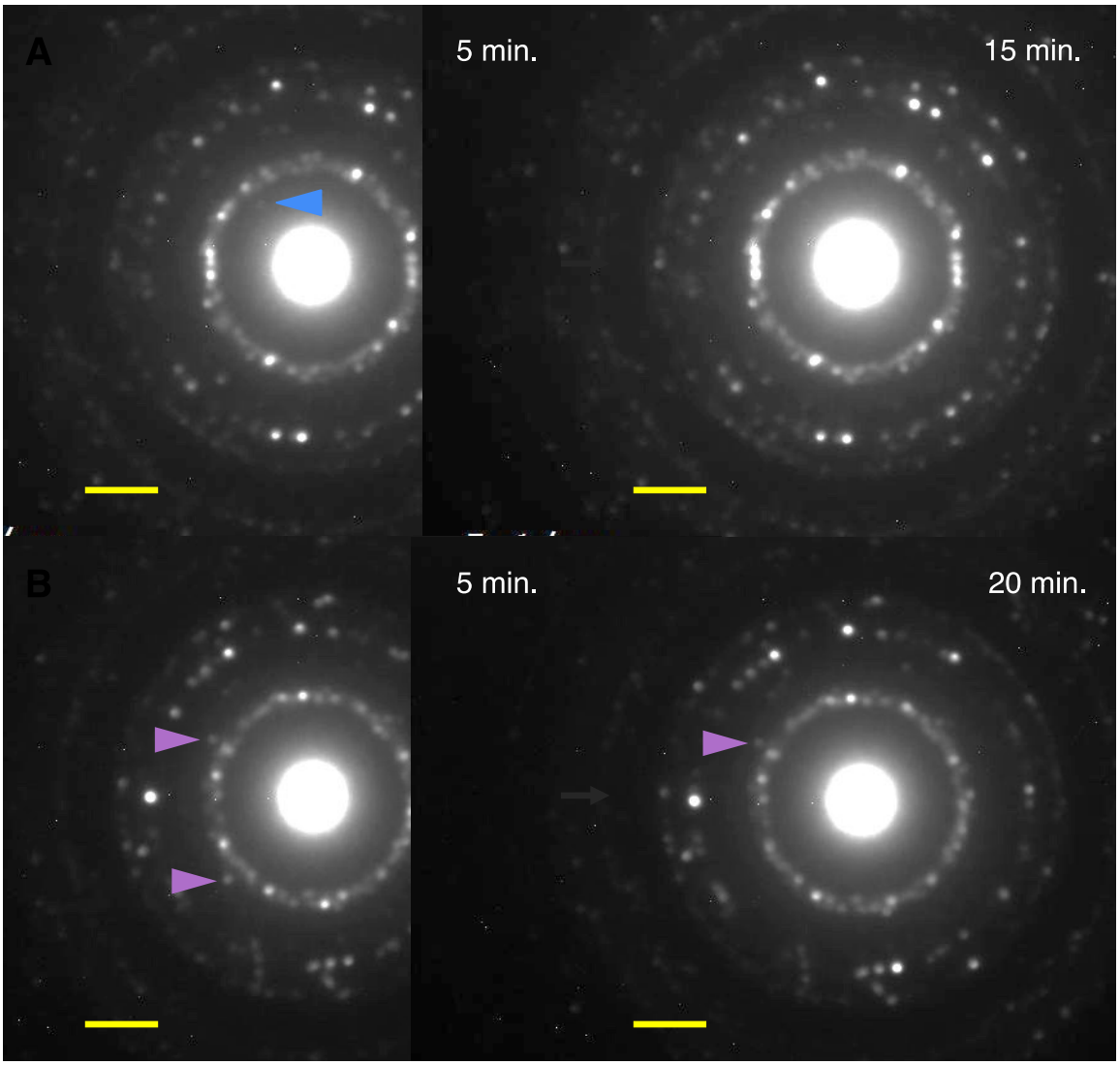

Figure 9. Disappearance of electron diffraction spots of hydrogen-ordered cubic ice with further electron irradiation. After 15-min electron irradiation, the Group D (d = 4.51 Å) diffraction spot (blue arrowhead in the 5-min irradiation pattern) weakened during annealing at 120 K (A). A Group E (d = 3.19 Å) diffraction spot (purple arrowhead) observed in the 5-min irradiation disappeared after the 20-min electron irradiation in the UV irradiation experiment at 130 K, but another diffraction spot remained (B). Yellow scale bars, 2 nm^{-1}.

The formation of hydrogen-ordered cubic ices by coarsening proceeded very slowly under the condition of very small supersaturation. Thus, we performed additional experiments to confirm

whether the ice was formed by slow deposition and crystallization of amorphous ice. During a slow deposition experiment at 120 K (Figure 10), we did not observe changes in the grain size (number density) or crystalline structure. However, afterward, coarsening and the appearance of hydrogen-ordered cubic ice were observed. The supersaturation, s, during deposition was defined as $s = (p - p_e)/p_e$, where p is the actual vapor pressure of H_2O and p_e is the equilibrium vapor pressure at 120 K calculated using vapor pressure formula of ice Ih[33] ; s was estimated to be $(10^{-6} - 5 \times 10^{-10})/(5 \times 10^{-10}) \sim 5 \times 10^3$. During the crystallization experiment of amorphous ice at 130 K (Figure 11), hydrogen-ordered cubic ice was not observed when crystallization was completed but was observed during coarsening. The supersaturation, s, during crystallization was defined as $s = L(T_m - T)/kT_mT$, where L is the latent heat of crystallization per molecule at 0 K[34], $T_m = 273$ K (melting point of ice), and $T = 130$ K; it was calculated to be 0.76. The estimation of the supersaturations of these two processes indicated that hydrogen-ordered cubic ice was not formed in such conditions far from equilibrium.

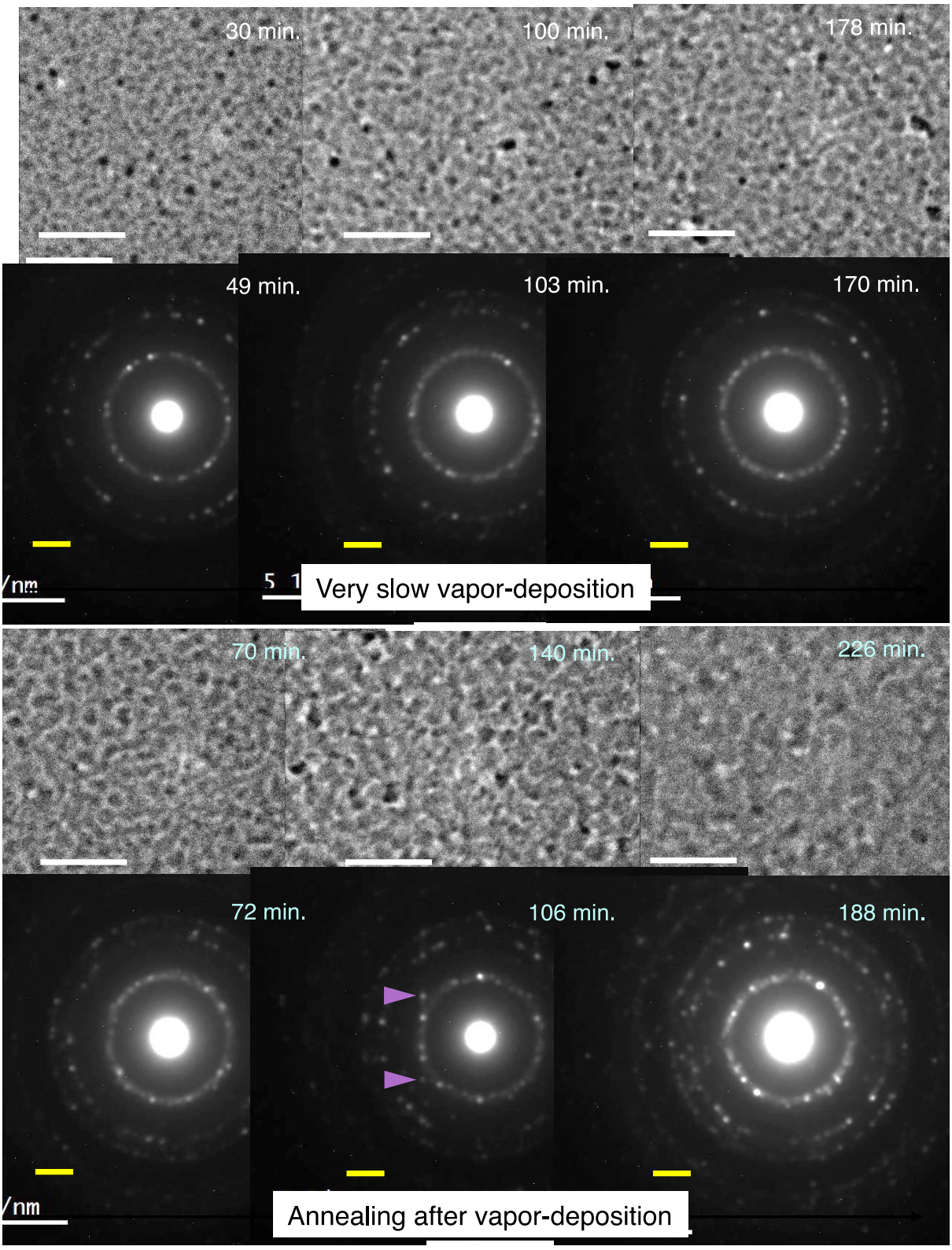
30 min.
100 min.
178 min.
49 min.
103 min.
170 min.
/nm
Very slow vapor-deposition
70 min.
140 min.
226 min.
72 min.
106 min.
188 min.
/nm
Annealing after vapor-deposition

Figure 10. Changes in TEM images and electron diffraction patterns during slow deposition followed by annealing at 120 K. First, small ice Ic crystals were formed by deposition at a rate of ~300 nm/h at 140 K for 1 min followed by cooling to 120 K for further slow deposition at a rate of ~15 nm/h for 3 h. The elapsed time during deposition and annealing is shown in each figure as white and pale blue numerals. White scale bars, 500 nm; yellow scale bars, 2 nm^{-1}.

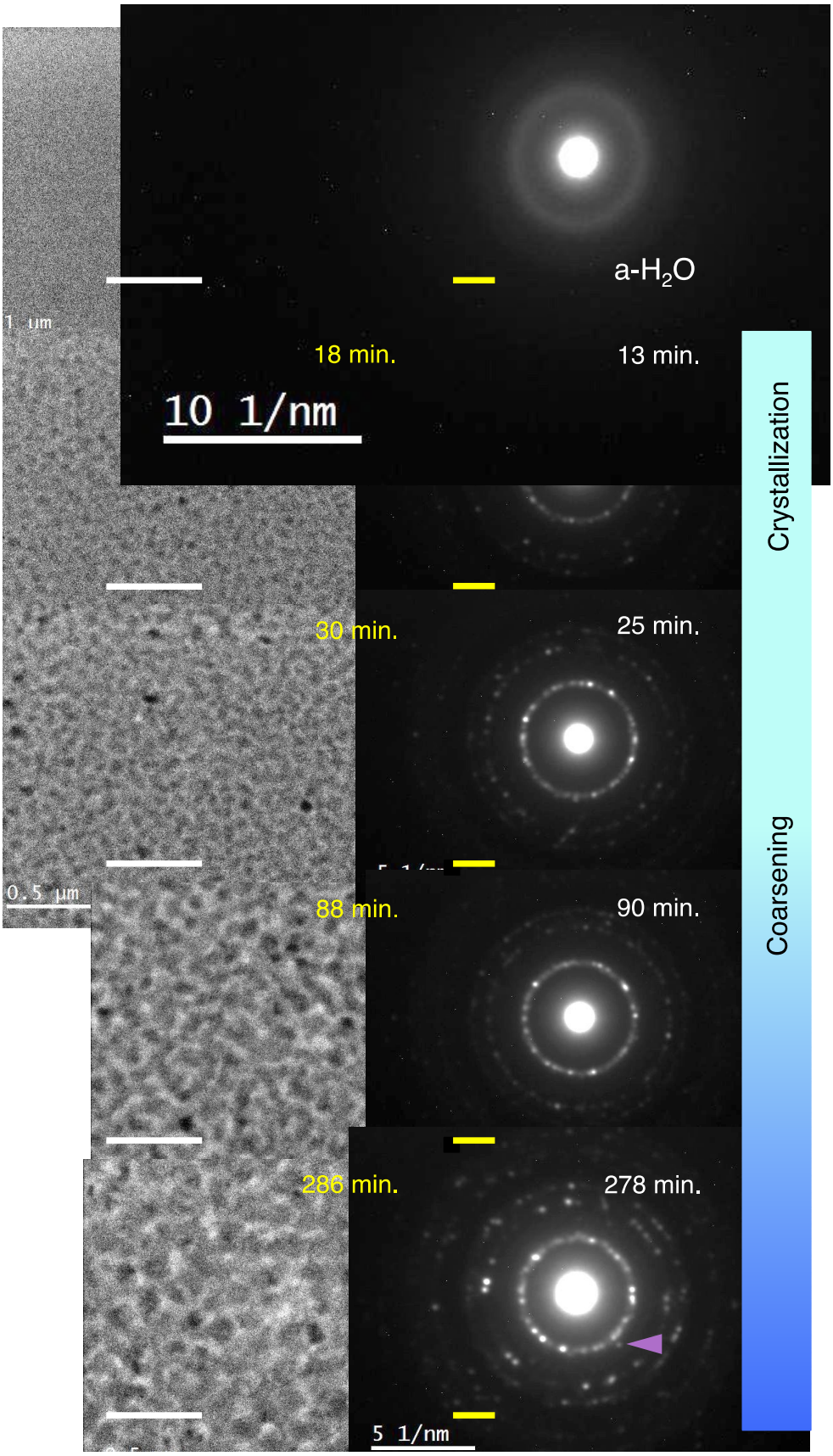
a-H2O
18 min.
13 min.
10 1/nm
1 µm
30 min.
25 min.
0.5 µm
88 min.
90 min.
286 min.
278 min.
5 1/nm
Crystallization
Coarsening

Figure 11. Changes in TEM images and electron diffraction patterns during crystallization of amorphous ice at 130 K. First, amorphous H_2O was deposited at 80 K and warmed to 130 K. The elapsed time during annealing is shown in each figure. White scale bars, 500 nm; yellow scale bars, 2 nm^{-1}.

The fraction of hydrogen-ordered cubic ices formed by UV irradiation is shown in Figure 8. Within 120–130 K, there was no difference between the annealing and UV irradiation experiments, indicating that UV irradiation did not affect the formation of hydrogen-ordered cubic ices. Conversely, we observed that hydrogen-ordered cubic ices were formed by UV irradiation at 100 K because the OH^- and OH radicals formed by UV irradiation were considered to increase the mobility of water molecules. The ratio of the hydrogen-ordered cubic ices observed in the UV irradiation experiments was Group A:Group B:Group C:Group E = 1:1:10:88, which was practically the same as that in the annealing experiments. A previous study observed the formation of ice XI via UV irradiation of ice Ih within 75–140 K.[22] Considering the present results, whether UV rays affected the formation of ice XI within 120–140 K was debatable. In addition, they performed only short-term (30–60 min) UV irradiation and annealing experiments. We strongly suggest that ice XI might be formed by long-term annealing of ice Ih within 120–140 K without irradiation or doping.

We now discuss the possible formation routes of hydrogen-ordered cubic ices in space (Figure 12). The first possibility is crystallization of amorphous ice. Interstellar grains in molecular clouds comprise a silicate core, an inner organic mantle, and an outer amorphous H_2O mantle. When the solar nebula was formed, these icy grains were heated and crystallized at approximately 90 K on a 10^5-year time scale[35] and were annealed. The main difference between the present study and the conditions in space is the kinds of substrates. Here, a-SiN was used,

whereas silicate or organics are involved in space. A study investigated the crystallization of amorphous ice on silicate and organics[36] and observed similar 3D islands, as shown in Figure 11. Therefore, hydrogen-ordered cubic ices can be formed on the surface of ice Ic by crystallization of amorphous ice and subsequent coarsening. The second possibility is condensation of ice crystals from the vapor phase. When the solar nebula cooled, condensation of ice Ic occurred in the Jovian region, resulting in the formation of hydrogen-ordered cubic ices on the surface of ice Ic by subsequent annealing. Formation of grains will occur in a gas flowing out of the surface of a giant star. Silicate grains will condense at approximately 1000 K, and ice Ic will condense on the silicate grains at approximately 100 K.[35] Similar to the solar nebula, hydrogen-ordered cubic ices will grow on the surface of ice Ic. Approximately half of hydrogen-ordered cubic ice is chiral (space groups: $P4_1$, $P2_1$, $P4_12_12$, and $P2_12_12$),[14,18] and the present results may have important implications for the origin of the homochirality of organic molecules in space.

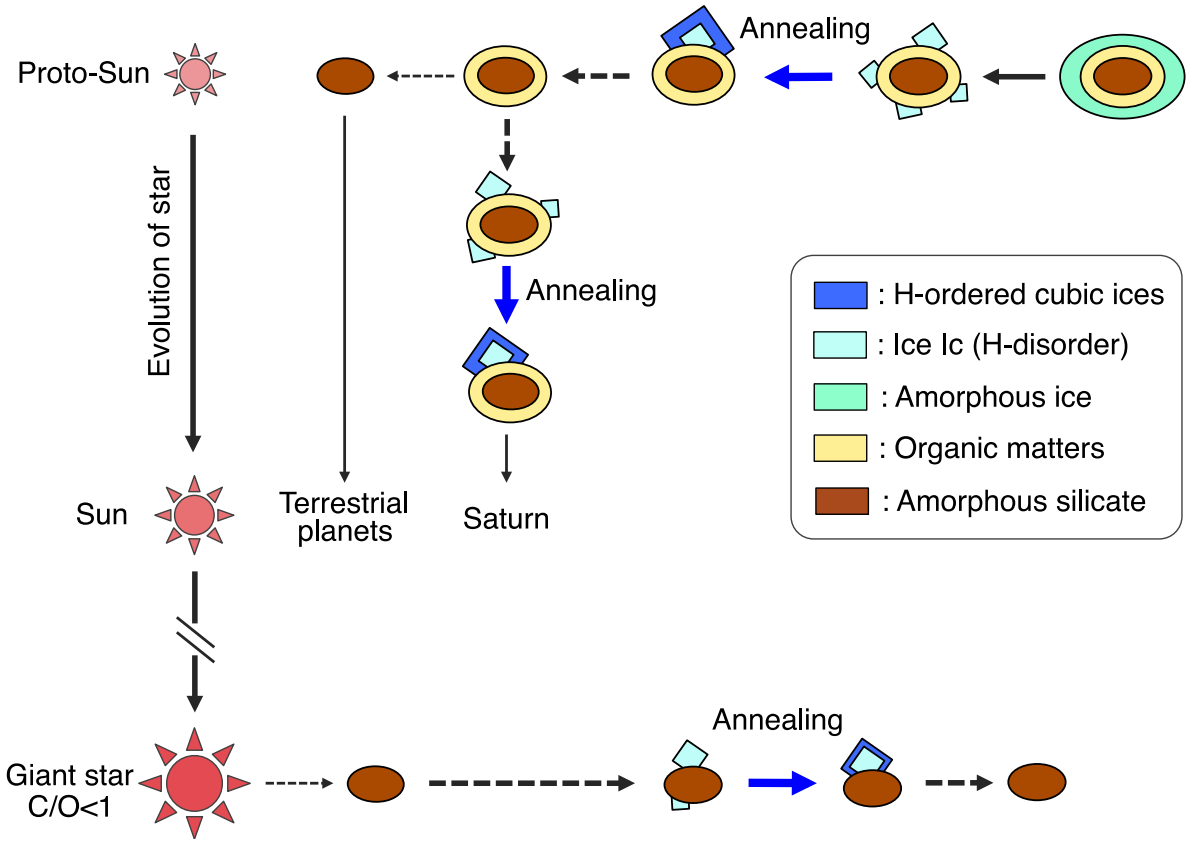

Figure 12. Schematic of the formation of hydrogen-ordered cubic ice in space. The evolution of icy grains is shown along with the evolution of the Sun. The respective colors show the structure of the water ice and composition of the refractory grains. The black broken arrows show the sublimation or condensation of H_2O ice. The blue solid arrows indicate the formation of hydrogen-ordered cubic ice.

CONCLUSION

A summary of the experiments is shown in Figure 13. As described, our novel method for formation of hydrogen-ordered cubic ices completely differs from that of ice XI. To realize hydrogen ordering at low temperatures (shorten the relaxation time of molecular movement in ice Ih), KOH doping[9-11] or high-energy electron irradiation[12] was applied to form OH^- in ice Ih. Conversely, the present method produced hydrogen-ordered cubic ices without doping or irradiation. The formation of discrete 3D islands of ice Ic and subsequent annealing were essential. Thus, hydrogen-ordered cubic ices can be formed on the surface of ice Ic by coarsening. At present, the formation mechanism of hydrogen-ordered cubic ices remains unknown, and we hope that it will be clarified in the near future. For the production of discrete 3D islands of ice Ic, direct deposition of ice Ic and crystallization of amorphous ice are acceptable. Another important factor is the selection of the substrate. For example, Pt(111), on which ice Ic epitaxially grows as uniform layers, was inadequate, but a-SiN, on which ice Ic does not epitaxially grow, was adequate. Furthermore, the surface diffusion coefficient on the substrate should be considered. Considering that the surface diffusion coefficient on the ice crystal was sufficiently large between 80 and 130 K,[37] the coefficient on the substrate should also be sufficiently large (Figure S2).

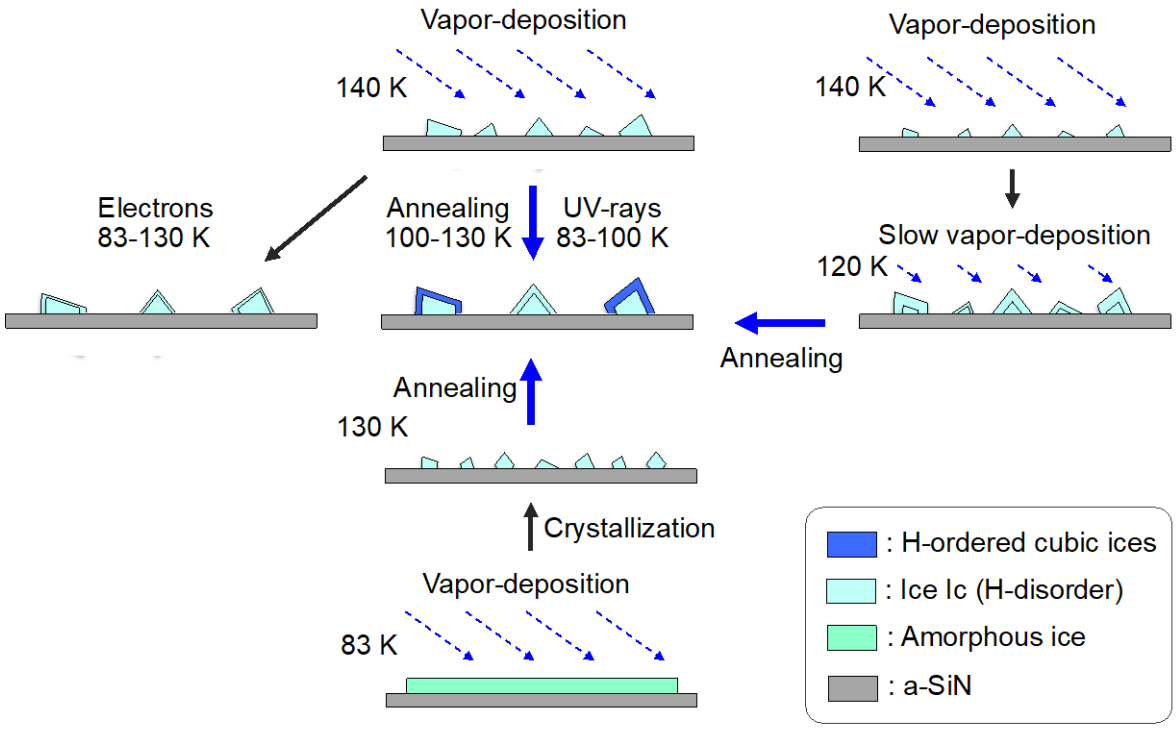

Figure 13. Summary of the present experiments. Five experiments were performed: vapor deposition of ice Ic at 140 K and subsequent annealing, UV irradiation or electron irradiation, extremely slow vapor deposition and subsequent annealing, and crystallization of amorphous ice and subsequent annealing. The blue thin dotted lines show vapor deposition, and their length indicates the deposition rate. The respective colors show the structure of the water ice. The blue solid arrows indicate the formation of hydrogen-ordered cubic ice, and the black solid arrows indicate no structural change in ice Ic.

ASSOCIATED CONTENT

Supporting Information

The structure of Isd (Figure S1), Surface diffusion coefficient of water molecules on the a-SiN substrate (Figure S2), TEM image after 6-h electron irradiation at 120 K (Figure S3), lattice constants of calculated ices (Table S1), and calculated relative intensities of hydrogen-ordered ices Ih (Table S2).

AUTHOR INFORMATION

***Corresponding Author**

Yuki Kimura

Institute of Low Temperature Science, Hokkaido University, Sapporo 060-0819, Japan; orcid.org/0000-0002-9218-7663

Telephone: +81-11-706-7666

Email: ykimura@lowtem.hokudai.ac.jp

Authors

Akira Kouchi – Institute of Low Temperature Science, Hokkaido University, Sapporo 060-0819, Japan; orcid.org/0000-0002-0495-5408

Tomoya Yamazaki – Institute of Low Temperature Science, Hokkaido University, Sapporo 060-0819, Japan; orcid.org/0000-0001-8190-3778

Hiroyasu Katsuno −Institute of Low Temperature Science, Hokkaido University, Sapporo 060-0819, Japan; orcid.org/0000-0002-2024-6919

Hiroki Nada – National Institute of Advanced Industrial Science and Technology (AIST), Tsukuba 305-8569, Japan; orcid.org/0000-0002-1744-2759

Tetsuya Hama – Komaba Institute for Science, The University of Tokyo, Tokyo 153-8902, Japan; orcid.org/0000-0002-4991-4044

Notes

The authors declare no competing financial interests.

ACKNOWLEDGMENTS

We thank Y. Seto of Osaka Metropolitan University for opening the ReciPro program. The authors thank two anonymous reviewers for constructive comments. This research was partly supported by Grants-in-Aid for Scientific Research from the Ministry of Education, Culture, Sports, Science, and Technology (grant JP25108002 and JP20H05849) and from the Japan Society for the Promotion of Science (grant JP20H05657).

REFERENCES

(1) Petrenko, V. F.; Whitworth, R. W. *Physics of Ice*; Oxford University Press, New York, 1999.

(2) Salzmann, C. G. Advances in the Experimental Exploration of Water's Phase Diagram. *J. Chem. Phys.* **2019**, *150*, 060901. DOI: 10.1063/1.5085163

(3) Yamane, R.; Komatsu, K.; Gouchi, J.; Uwatoko, Y.; Machida, S.; Hattori, T.; Ito, H.; Kagi, H. Experimental Evidence for the Existence of a Second Partially-Ordered Phase of Ice VI. *Nat. Commun.* **2021**, *12*, 1129. DOI: 10.1038/s41467-021-21351-9

(4) Prakapenka, V. B.; Holtgrewe, N.; Lobanov, S. S.; Goncharov, A. F. Structure and Properties of Two Superionic Ice Phases. *Nat. Phys.* **2021**, *17*, 1233–1238. DOI: 10.1038/s41567-021-01351-8

(5) Gasser, T. M.; Thoeny, A. V.; Fortes, A. D.; Loerting, T. Structural characterization of ice XIX as the second polymorph related to ice VI. *Nat. Commun.* **2021**, *12*, 1228. DOI: 10.1038/s41467-021-21161-z

(6) Salzmann, C. G.; Loveday, J. S.; A. Craig R-F.; Bull, L. Structure and nature of ice XIX. *Nat. Commun.* **2021**, *12*, 3162. DOI: 10.1038/s41467-021-23399-z

(7) Engel, E. A.; Anelli, A.; Ceriotti, M.; Pickard, C. J.; Needs, R. J. Mapping uncharted territory in ice from zeolite networks to ice structures. *Nat. Commun.* **2018**, *9*, 2173. DOI: 10.1038/s41467-018-04618-6

(8) Nada, H. Pathways for the formation of ice polymorphs from water predicted by a metadynamics method. *Sci. Rep.* **2020**, *10*, 4708. DOI: 10.1038/s41598-020-61773-x

(9) Kawada, S. Dielectric Dispersion and Phase Transition of KOH Doped Ice. *J. Phys. Soc. Jpn.* **1972**, *32*, 1442. DOI: 10.1143/JPSJ.32.1442

(10) Tajima, Y.; Matsuo, T.; Suga, H. Phase Transition in KOH-Doped Hexagonal Ice. *Nature* **1982**, *299*, 810–812. DOI: 10.1038/299810a0

(11) Leadbetter, A. J.; Ward, R. C.; Clark, J. W.; Tucker, P. A.; Matsuo, T.; Suga, H. The Equilibrium Low Temperature Structure of Ice. *J. Chem. Phys.* **1985**, *82*, 424–428. DOI: 10.1063/1.448763

(12) Kobayashi, K.; Yasuda, H. Phase Transition of Ice Ic to Ice XI Under Electron Beam Irradiation. *Chem. Phys. Lett.* **2012**, *547*, 9–12. DOI: 10.1016/j.cplett.2012.07.076

(13) Salzmann, C. G.; Radaelli, P. G.; Slater, B.; Finney, J. L. The Polymorphism of Ice: Five Unresolved Questions. *Phys. Chem. Chem. Phys.* **2011**, *13*, 18468–18480. DOI: 10.1039/c1cp21712g

(14) Geiger, P.; Dellago, C.; Macher, M.; Franchini, C.; Kresse, G.; Bernard, J.; Stern, J. N.; Loerting, T. Proton Ordering of Cubic Ice Ic: Spectroscopy and Computer Simulations. *J. Phys. Chem. C Nanomater. Interfaces* **2014**, *118*, 10989–10997. DOI: 10.1021/jp500324x

(15) Minagawa, I. Phase Transition of Cubic Ice Ic. *J. Phys. Soc. Jpn.* **1985**, *54*, 1610–1614. DOI: 10.1143/JPSJ.54.1610

(16) Lekner, J. Electrostaticss of Proton Arrangements in Ice Ic. *Phys. B Condens. Matter* **1997**, *240*, 263–272. DOI: 10.1016/S0921-4526(97)00430-4

(17) Casassa, S.; Calatayud, M.; Doll, K.; Minot, C.; Pisani, C. Proton Ordered Cubic and Hexagonal Periodic Models of Ordinary Ice. *Chem. Phys. Lett.* **2005**, *409*, 110–117. DOI: 10.1016/j.cplett.2005.04.068

(18) Raza, Z.; Alfè, D.; Salzmann, C. G.; Klimeš, J.; Michaelides, A.; Slater, B. Proton Ordering in Cubic Ice and Hexagonal Ice; A Potential New Ice Phase—XIc. *Phys. Chem. Chem. Phys.* **2011**, *13*, 19788–19795. DOI: 10.1039/C1CP22506E

(19) Engel, E. A.; Monserrat, B.; Needs, R. J. Anharmonic Nuclear Motion and the Relative Stability of Hexagonal and Cubic Ice. *Phys. Rev. X* **2015**, *5*, 021033. DOI: 10.1103/PhysRevX.5.021033

(20) Yuan, Z. Y.; Zhang, P.; Yao, S. K.; Lu, Y. B.; Yang, H. Z.; Luo, H. W.; Zhao, Z. J. Computational Assignments of Lattice Vibrations of Ice Ic. *RSC Adv.* **2017**, *7*, 36801–36806. DOI: 10.1039/C7RA04332E

(21) Yamamuro, O.; Oguni, M.; Matsuo, T.; Suga, H. Heat Capacity and Glass Transition of Pure and Doped Cubic Ices. *J. Phys. Chem. Solids* **1987**, *48*, 935–942. DOI: 10.1016/0022-3697(87)90130-2

(22) Kouchi, A.; Kimura, Y.; Kitajima, K.; Katsuno, H.; Hidaka, H.; Oba, Y.; Tsuge, M.; Yamazaki, T.; Fujita, K.; Hama, T.; et al. UV-Induced Formation of Ice XI Observed Using an Ultra-High Vacuum Cryogenic Transmission Electron Microscope and Its Implications for Planetary Science. *Front. Chem.* **2021**, *9*, 799851. DOI: 10.3389/fchem.2021.799851

(23) Brown, D. E.; George, S. M.; Huang, C.; Wong, E. K. L.; Rider, K. B.; Smith, R. S.; Kay, B. D. H_2O Condensation Coefficient and Refractive Index for Vapor-Deposited Ice from Molecular Beam and Optical Interference Measurements. *J. Phys. Chem.* **1996**, *100*, 4988–4995. DOI: 10.1021/jp952547j

(24) Seto, Y.; Ohtsuka, M. ReciPro: Free and Open-Source Multipurpose Crystallographic Software Integrating a Crystal Model Database and Viewer, Diffraction and Microscopy Simulators, and Diffraction Data Analysis Tools. *J. Appl. Crystallogr.* **2022**, *55*, 397–410. DOI: 10.1107/S1600576722000139

(25) Hirsch, T. K.; Ojamäe, L. Quantum-Chemical and Force-Field Investigation of Ice Ih: Computation of Proton-Ordered Structures and Prediction of Their Lattice Energies. *J. Phys. Chem. B* **2004**, *108*, 15856–15864. DOI: 10.1021/jp048434u

(26) Malkin, T. L.; Murray, B. J.; Salzmann, C. G.; Molinero, V.; Pickering, S. J.; Whale, T. F. Stacking Disorder in Ice I. *Phys. Chem. Chem. Phys.* **2015**, *17*, 60–76. DOI: 10.1039/c4cp02893g

(27) del Rosso, L.; Celli, M.; Grazzi, F.; Catti, M.; Hansen, T. C.; Fortes, A. D.; Ulivi, L.; Cubic ice Ic without stacking defects obtained from ice XVII. *Nat. Mater.* **2020**, *19*, 663–668. DOI: 10.1038/s41563-020-0606-y

(28) Komatsu, K.; Machida, S.; Noritake, F.; Hattori, T.; Sano-Furukawa, A.; Yamane, R.; Yamashita, K.; Kagi, H.; Ice I_c without stacking disorder by evacuating hydrogen from hydrogen hydrate. *Nat. Commun.* **2020**, *11*, 464. DOI: 10.1038/s41467-020-14346-5

(29) Salzmann, C. G., Murray, B. J. Ice goes fully cubic. *Nat. Mater.* **2020**, *19*, 586–587. DOI: 10.1038/s41563-020-0696-6

(30) Rosu-Finsen, A.; Chikani, B.; Salzmann, C. G.; Thermal desorption of H_2O ice: from nanoscale films to the bulk. *Mon. Notices Royal Astron. Soc.* **2022**, 517, 1919-1927. DOI: 10.1093/mnras/stac2803

(31) Bertie, J. E.; Calvert, L. D.; Whalley, E. Transformations of Ice II, Ice III, and Ice V at Atmospheric Pressure. *J. Chem. Phys.* **1963**, *38*, 840–846. DOI: 10.1063/1.1733772

(32) Kuhs, W. F.; Sippel, C.; Falenty, A.; Hansen, T. C. Extent and Relevance of Stacking Disorder in "Ice Ic". *Proc. Natl. Acad. Sci. U. S. A.* **2012**, *109*, 21259–21264. DOI: 10.1073/pnas.1210331110

(33) Mauersberger, K.; Krankowsky, D. Vapor pressure above ice at temperatures below 170 K. *Geophys. Res. Lett.* **2003**, *30*, 21. DOI: 10.1029/2002GL016183

(34) Ghormley, J. A. Enthalpy Changes and Heat-Capacity Changes in the Transformations from High-Surface-Area Amorphous Ice to Stable Hexagonal Ice. *J. Chem. Phys.* **1968**, *48*, 503- DOI: 10.1063/1.1667954

(35) Kouchi, A.; Yamamoto, T.; Kozasa, T.; Kuroda, T.; Greenberg, J. M. Conditions for Condensation and Preservation of Amorphous Ice and Crystallinity of Astrophysical Ices. *Astron. Astrophys.* **1994**, *290*, 1009–1018.

(36) Kouchi, A.; Tsuge, M.; Hama, T.; Oba, Y.; Okuzumi, S.; Sirono, S. I.; Momose, M.; Nakatani, N.; Furuya, K.; Shimonishi, T.; et al. Transmission Electron Microscopy Study of the Morphology of Ices Composed of H_2O, CO_2, and CO on Refractory Grains. *Astrophys. J.* **2021**, *918*, 45. DOI: 10.3847/1538-4357/ac0ae6

(37) Kiefer, J.; Hale, B. N. The Water Monomer on the Basal Plane of Ice I_h: An Effective Pair, Central Force Potential Model of the Static Interaction. *J. Chem. Phys.* **1977**, *67*, 3206–3213. DOI: 10.1063/1.435235

(38) Kouchi, A.; Furuya, K.; Hama, T.; Chigai, T.; Kozasa, T.; Watanabe, N. Direct Measurements of Activation Energies for Surface Diffusion of CO and CO_2 on Amorphous Solid Water Using In Situ Transmission Electron Microscopy. *Astrophys. J. Lett.* **2020**, *891*, L22. DOI: 10.3847/2041-8213/ab78a2